Inversion of TE experimental data using the distorted Born iterative method

***Puyan Mojabi* and Joe LoVetri**

E2-290 Engineering Building, University of Manitoba, Winnipeg, MB, R3T 5V6, Canada.
Tel. 204-474-9835, Fax. 204-261-4639.
pmojabi@ee.umanitoba.ca, lovetri@ee.umanitoba.ca

Abstract

We apply the Distorted Born Iterative Method (DBIM) for the inversion of Transverse Electric (TE) experimental data provided by Institut Fresnel, both for single- and multiple-frequency cases. The results show that the DBIM applied to TE inversion does not converge as well as when it is applied to Transverse Magnetic (TM) inversion for the cases considered herein.

1. Introduction

Most of the inverse scattering algorithms that have been tested against two-dimensional '*experimental*' data consider the Transverse Magnetic (TM) case because it can be formulated as a scalar problem. Only a few reports on the inversion of the Transverse Electric (TE) '*experimental*' data have been published; in the first special edition on Fresnel experimental data set [1], only one paper considered the inversion of TE-polarized data to reconstruct the permittivity distribution of the object [2]. In the second special edition on Fresnel experimental data [3-4], only one paper showed the inversion of TE-polarized data using a TE inversion algorithm [5]. Both of these two publications used the Multiplicative Regularized Contrast Source Inversion (MR-CSI) method to invert the TE-polarized data. These two works showed multiple-frequency reconstructions and did not provide single-frequency reconstruction results.

To the best of our knowledge, the inversion of TE '*experimental*' data using the Distorted Born Iterative Method (DBIM) [6] has not been published. Previously published work on the TE inversion using the DBIM are based on synthetic data, see for example [7-8]. Herein, we show single-frequency and multiple-frequency results of using the DBIM algorithm to invert the TE experimental data collected by the researchers at Institut Fresnel, France which is freely provided to the inverse community [3].

2. Formulation of the problem

The objects considered in the experimental data are very large in the direction which is perpendicular to the plane where transmitter and receivers antennas are located; therefore, justifying the use of two-dimensional inversion algorithms. Assuming the cylindrical object with an arbitrary inhomogeneous cross section in the $x-y$ plane and invariant in the z direction, we consider a two-dimensional imaging domain $D \subset \mathbb{R}^2$ containing the cross section of the object(s) and a measurement surface $S \subset \mathbb{R}^2 \backslash \mathrm{D}$. The complex electric contrast can be defined as a function of position $\boldsymbol{q}$ as $\chi(\boldsymbol{q}) = (\varepsilon(\boldsymbol{q}) - \varepsilon_b(\boldsymbol{q}))/(\varepsilon_b(\boldsymbol{q}))$ where $\varepsilon_b(\boldsymbol{q})$ is the background permittivity which can be an inhomogeneous complex quantity. Here, we try to reconstruct χ inside D from the measured scattered field on S, which is outside D, due to some known TE-polarized incident fields.

Assuming such TE illumination, the total electric field can be represented as a two-component vector, $\boldsymbol{E} = E_x\hat{x} + E_y\hat{y}$, in the cross section of the object. Assuming the scattered electric field is $\boldsymbol{E}^{sct} = \boldsymbol{E} - \boldsymbol{E}^{inc}$, and the wave-number of the background medium $k_b(\boldsymbol{q}) = \sqrt{\omega^2\mu_b\varepsilon_b(\boldsymbol{q})}$, the integral formulation of the so-called *data equation* is written as

$$\boldsymbol{E}^{sct}(\boldsymbol{p}) = \int_{q \in D} k_b^2(\boldsymbol{q})\overline{G}(\boldsymbol{p}, \boldsymbol{q}) \bullet \chi(\boldsymbol{q})\boldsymbol{E}(\boldsymbol{q})dv(\boldsymbol{q}), \ \boldsymbol{p} \in S \tag{1}$$

where $\overline{G}(\boldsymbol{p}, \boldsymbol{q})$ is the dyadic Green's function for the background medium. The *data equation* is an ill-posed Fredholm integral equation of the first kind with unknowns $\chi(\boldsymbol{q} \in D)$ and $\boldsymbol{E}(\boldsymbol{q} \in D)$ which are nonlinearly related via the well-posed *domain equation* given as

$$\boldsymbol{E}^{inc}(\boldsymbol{p}) = \boldsymbol{E}(\boldsymbol{p}) - \int_{\boldsymbol{q} \in D} k_b^2(\boldsymbol{q})\overline{G}(\boldsymbol{p}, \boldsymbol{q}) \bullet \chi(\boldsymbol{q})\boldsymbol{E}(\boldsymbol{q})dv(\boldsymbol{q}), \boldsymbol{p} \in D. \tag{2}$$

We solve (1) for the contrast χ using the DBIM which tries to iteratively cast this nonlinear ill-posed problem to a linear Fredholm integral equation of the first kind at each iteration. The total field inside the imaging domain, the background medium and its corresponding Green's function are updated in each iteration. The total field inside the imaging domain and the Green's function are updated via a forward solver using the Conjugate Gradient technique with Fast Fourier Transform (CG-FFT). Our implementation is similar to that described in [9]. To further accelerate the convergence of the conjugate gradient technique, we used the *marching-on-in-source-position* technique for both updating the total field and the Green's function [10, 11]. The ill-posedness of the linearized inverse problem is treated using Tikhonov regularization. Assuming the discrete representations of the ill-posed operator, the measured data, the unknown contrast and the Laplacian operator are denoted as $\boldsymbol{A}$, $\boldsymbol{b}$, $\boldsymbol{x}$ and $\boldsymbol{L}$, respectively, then at each iteration, we find $\boldsymbol{x}$ by minimizing $\|\boldsymbol{b} - \boldsymbol{A}\boldsymbol{x}\|_2^2 + \lambda^2\|\boldsymbol{L}\boldsymbol{x}\|_2^2$ where λ is the regularization parameter. Here, λ is determined using a fast implementation of the *L*-curve which does not require Singular Value Decomposition (SVD) [12].

3. Results and conclusion

The transmitting and receiving antennas for the Fresnel experimental setup are both wide-band ridged horn antennas and are located in a circle with radius 1.67m. The objects under test are all long circular cylinders having a height of 1.50m and having no variations in the longitudinal direction. All of the objects are combinations of a large cylinder with contrast $\chi_1 = 0.45 \pm 0.15$ and a small cylinder with contrast $\chi_2 = 2 \pm 0.3$. Both TE and TM polarizations are measured for each target. The measured scattered field is then calibrated according to [2]. For the results shown in this paper, the imaging domain, D, is considered to be a $15\text{cm} \times 15\text{cm}$ square which is discretized into 60×60 squares upon which the dielectric contrast is assumed to be constant. For single-frequency reconstructions, we have used the Born approximation as the initial guess to the DBIM. For the multiple-frequency inversion results, we have used the frequency-hopping approach. Reconstruction results for all three lossless dielectric objects in the Fresnel data set are shown in Figure 1 while the reconstruction of the profile containing the metal, *i.e. FoamMetExt*, has not been shown because the TE inversion using the DBIM did not converge to a meaningful solution (note that the TM inversion using the same implementation of the DBIM converged successfully).

SINGLE-FREQUENCY RECONSTRUCTION AT $f = 2$ GHz. In the cases considered herein, the reconstructed contrast of the small cylinder does not reach the true contrast which is $\chi_2 = 2.0 \pm 0.3$. It has been speculated by Otto and Chew [7] that the poor convergence performance of the DBIM for the TE case is likely due to the presence of polarization charges at dielectric discontinuities. These induced charges, which don't exist in TM polarization, partially mask the scattering effect of the object and increase the nonlinearity of the problem [7]. Also, because of the strong effect of the polarization charges on the surface of the metallic copper in *FoamMetExt*, the DBIM was not able to reconstruct this profile from TE-polarized data (TM inversion was successful in this profile). In order for the DBIM to converge to the true solution, it is important that the initial guess used in the algorithm model the physics of the problem well. The Born approximation, which is our initial guess to the DBIM TE problem, poorly models the effects of induced polarized charges [7] and is therefore another reason for the poor convergence. It may be that with a better initial guess, the DBIM could converge to the true solution in single-frequency TE inversion. Note that, in TM single-frequency reconstruction using the same implementation of the DBIM, not shown here, the solution converges to the true profile.

MULTIPLE-FREQUENCY RECONSTRUCTION. For the three objects being considered, the scattered data are collected at 9 different frequencies from $f = 2$ GHz to $f = 10$ GHz with the step of 1 GHz. We've used the frequency-hopping technique to reconstruct the contrast using all the frequency data available. The reconstructed shape and location are satisfactory but the permittivity reconstruction is not good: there are some strong peaks in the

reconstruction of the '*external*' small cylinder although the average value of the permittivity distribution is close to that of the true profile. We speculate that this is likely due to the fact that the interfacial charges shield the inner part of the cylinder such that the DBIM algorithm underestimates the contrast of the object in some parts. The DBIM then compensates for this by overestimating the contrast at some other points in the neighborhood of the points where the contrast was underestimated. Note that these strong peaks are not present in the reconstruction of the '*inner*' small cylinder in *FoamDielInt* and *FoamTwinDiel* as the dielectric discontinuity between the inner small cylinder and the outer large cylinder is less than that of the external small cylinder and the background medium. The TM multiple-frequency reconstruction of all the Fresnel objects using the DBIM was successful.

In conclusion, the DBIM applied to TE inversion does not perform as well as when it is used for TM inversion for the same Fresnel objects. Comparing these TE reconstructions with the results obtained by the MR-CSI method [5] shows that the MR-CSI method out-performs the DBIM in all these cases. We surmise that the MR-CSI produces better results due to the fact that is not based on the linearization of the inverse scattering problem.

4. References

1. K. Belkebir and M. Saillard, "Special section: testing inversion algorithms against experimental data," *Inverse Probl.*, **17**, 2001, pp. 1565-157.

2. R. F. Bloemenkamp, A. Abubakar, and P. M. van den Berg, "Inversion of experimental multi-frequency data using the contrast source inversion method," *Inverse Probl.*, **17**, 2001, pp. 1611-1622.

3. J-M. Geffrin, P. Sabouroux and C. Eyraud, "Free space experimental scattering database continuation: experimental set-up and measurement precision," *Inverse Probl.*, **21**, 2005, S117-S130.

4. K. Belkebir and M. Saillard, "Testing inversion algorithms against experimental data: inhomogeneous targets," *Inverse Probl.*, **21**, 2005, S1-S3.

5. A. Abubakar, P. M. van den Berg and T. M. Habashy, "Application of the multiplicative regularized contrast source inversion method on TM- and TE-polarized experimental Fresnel data," *Inverse Probl.*, **21**, 2005, S5-S13.

6. W. C. Chew and Y. M. Wang, "Reconstruction of two-dimensional permittivity distribution using the distorted Born iterative method," *IEEE Trans. Med. Imaging*, **9**, 1990, pp. 218-225.

7. G. P. Otto and W. C. Chew, "Inverse scattering of H_z waves using local-shape function imaging: a T-matrix formulation," *Int. J. Imag. Syst. Technol.*, **5**, 1994, pp. 22-27.

8. J. Ma, W. C. Chew, C-C Lu and J. Song, "Image reconstruction from TE scattering data using equation of strong permittivity fluctuation," *IEEE Trans. Antennas Propag.*, **48**, 2000, pp. 860-867.

9. A. Abubakar and P. M. van den Berg, "Iterative forward and inverse algorithms based on domain integral equations for three-dimensional electric and magnetic objects," *Journal of Computational Physics*, **195**, 2004, pp. 236-262.

10. J. De Zaeytijd, A. Franchois, C. Eyraud and J-M Geffrin, "Full-wave three-dimensional microwave imaging with a regularized Guass-Newton method - theory and experiment," *IEEE Trans. Antennas Propag.*, **55**, 2007, pp. 3279-3292.

11. Z. Q. Peng and A. G. Tijhuis, "Transient scattering by a lossy dielectric cylinder: Marching-on-in-frequency approach," *J. Electrom. Waves Applic.*, **7**, 1993, pp. 739-763.

12. Calvetti, D., P. C. Hansen and L. Reichel, "*L*-curve curvature bounds via Lanczos bidiagonalization," *Electronic Transactions on Numerical Analysis*, **14**, 2002, pp. 20-35.

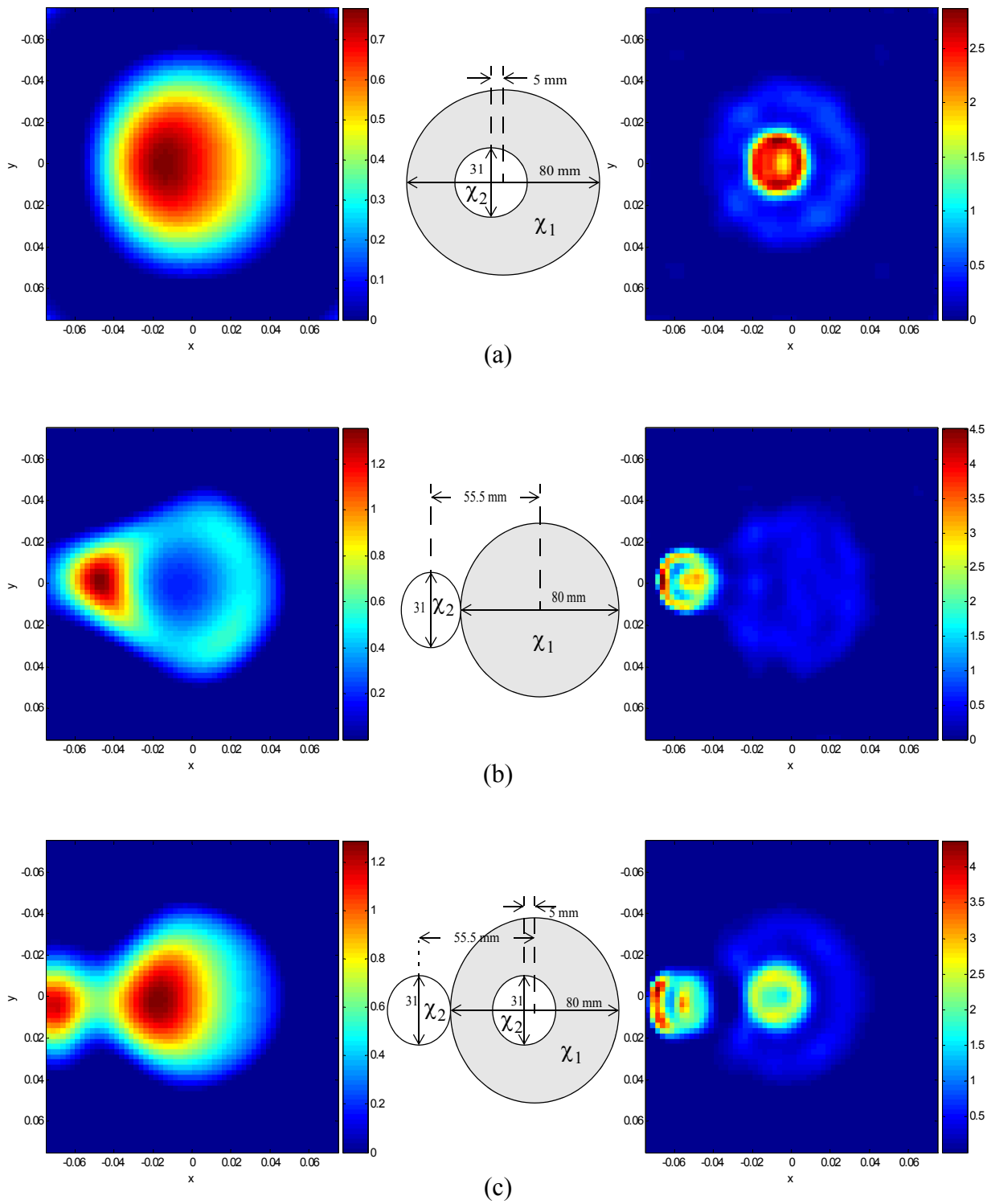

Figure 1 . (a) *FoamDielInt* (b) *FoamDielExt* (c) *FoamTwinDiel*
Left column: single-frequency reconstruction, middle column: true profile, right column: multiple-frequency reconstruction.